Hindawi
Advances in Meteorology
Volume 2022, Article ID 6971110, 16 pages
https://doi.org/10.1155/2022/6971110

Research Article

The Space Conceptual Models and Water Vapor Characteristics of Typical Rainstorms during Plum Rain Season

Ying Tian,[1,2] **Rong Yao**,[3] **Enrong Zhao**,[3] **Qian Yao**,[4] **and Xiaolong Pan**[3]

[1]*Shandong Key Laboratory of Meteorological Disaster Prevention and Reduction, Jinan 250031, China*
[2]*Shandong Meteorological Observatory, Jinan 250031, China*
[3]*Hunan Meteorological Observatory, Changsha 410018, China*
[4]*Hunan Meteorological Agency Service Center, Changsha 410118, China*

Correspondence should be addressed to Rong Yao; 543828780@qq.com

Received 10 January 2022; Revised 16 August 2022; Accepted 5 September 2022; Published 26 September 2022

Academic Editor: Yaolin Lin

Based on conventional observation data from the China Meteorological Administration (CMA) and reanalysis data from the American National Centers for Environmental Prediction and National Center for Atmospheric Research (NCEP/NCAR) between 2012 and 2021, combined with the meteorological analysis, composite synthesis, and water vapor trajectory analysis, the weather circulations of typical rainstorms during the 10 years can be divided into 4 categories: Static Front Pattern (SFP), Subtropical High Edge Pattern (SHEP), Northeast Cold Vortex Pattern (NCVP), and Low-Level Vortex and Shear Pattern (LLVSP). The SHEP and SFP rainstorms have the characteristics of long duration and wide range, while the NCVP rainstorms are characterized by mobility and disaster weather accompaniment. The daily precipitation of LLVSP cases has extremity feature. The occurrence and development of rainstorms are well coordinated with the systems on lower levels. The main water vapor channel in lower layers of the SFP cases is from the South China Sea, while it is from Bohai for the NCVP cases and the Bay of Bengal for the SHEP and LLVSP cases. The main water vapor channel in middle layers is from the Bay of Bengal because of the affection of the southwest air flow. The south boundary of the MLYRB is the most important water vapor input boundary, followed by the west boundary, while the East and North boundaries are the outflow boundaries. During the rainstorms, the low-level water vapor is exuberant with low-level water vapor convergence much stronger than the high-level divergence. Among the four types of rainstorms, the NCVP cases provide the most abundant low-level water vapor convergence, resulting in the strongest short-term precipitation among the four types. Combined with water vapor transportation and convergence, the refined spatial conceptual models of the four types of rainstorms can better judge the process intensity and falling area and provide reference for disastrous weather forecast and early warning.

1. Introduction

The Meiyu, which refers to the unique rainy season in the East Asian summer monsoon (EASM) region in late spring and early summer, is the second stationary period of the EASM [1–4]. The amount of precipitation and the location of the rain belt it produces are highly correlated with the flood or drought related conditions over the MLYRB [3, 5–7]. Therefore, it is of great significance for social and economic activities to study the causes of Meiyu [8–11].

Meiyu is the product of the interaction of tropical, subtropical, and mid-high latitude weather systems [9, 12–15]. Its atmospheric circulation is extremely complex with different scales in space and time. Meteorologists have done a lot of research from the aspects of climate statistics [16–19], large-scale circulation anomalies [10, 11, 20–27], rainstorm formation mechanisms [28–34], and so on.

The Meiyu processes in the MLYRB generally have typical weather situations [35, 36]. Through the classification of the influencing systems of rainstorm cases, it is helpful to understand the synoptic scale mechanisms that lead to rainstorms, so as to improve the prediction accuracy of such events. Tao [37] summarized various circulation patterns of persistent heavy rain in China and pointed out that the

stability of weather circulation, the transmission and convergence of water vapor, and the release and regeneration of convective unstable energy were the three basic conditions for the occurrence of persistent heavy rain in China. Maddox [38] investigated the temporal and spatial characteristics of 151 flash floods in the United States and divided these cases into four weather types according to the ground and upper air situation. Chen et al. [39] studied 117 heavy rainfall cases in Hunan from 2006 to 2014, which were divided into six types according to the experience and methods of rainstorm prediction in Hunan Province. According to the different triggering conditions of rainstorms, Deng et al. [40] established five conceptual models, including cold front type, static front type, and mesoscale trapped type. However, there are no classification studies on the impact systems of the MLYRB rainstorms during plum rain season yet, so this work has research significance.

Due to the great damage of rainstorms in the MLYRB in plum rain season, the analysis of water vapor source and transportation characteristics is also an important research aspect [41–44]. There is a direct relationship between water vapor convergence and precipitation in rainstorm area [41]. The lifting and condensation of wet air can make the low level jet (LLJ) rise to a higher altitude [37], and water vapor condensation can enhance the vertical movement in the frontal area significantly [45]. Numerical experiments show that if the high humidity center in the Indian Ocean and the Bay of Bengal weakens in the initial field, the precipitation in the MLYRB will decrease [42, 43]. Precipitation is sensitive to the initial value of water vapor on 850 hPa [46], and the release of latent heat during water vapor condensation is helpful to the triggering of new strong convection activities and increases precipitation [47]. While the water vapor in the upper troposphere has little influence on precipitation intensity and rain belt distribution, the water vapor in the middle layers plays an important role in maintaining the overall rain belt shapes, and the water vapor intensity change in the lower layers mainly affects the precipitation intensity in the center of the heavy rain. The closer the water vapor transmission position is to the shear line, the more conducive it is to the occurrence and development of the heavy rainfall [44].

Many research works on water vapor sources show that the main water vapor sources of summer rainstorms in the East China are the Bay of Bengal, the South China Sea, and the warm pool area of the Western Pacific [3, 48–51]. The studies above on water vapor sources and transportation are based on the Euler method, which cannot quantitatively distinguish the contribution of each water vapor source on precipitation. There are also some differences between the Euler flow field and the real trajectory of the air mass [52]. In consideration of the fact that the Lagrangian method can provide details and changes of water vapor along the water vapor transport trajectory, some scholars have applied this method to study the water vapor source and budget of rainstorms in recent years [53–62]. By tracking the three-dimensional position of every air block backward, this method determines the three-dimensional position and the physical quantities such as temperature, pressure, wind, and humidity of every air block at each time and defines the water vapor source contribution in the process of water vapor transportation. Currently, this method is widely used on a global scale [63] and in various subregions (the United States [64, 65], Europe [66–68], Latin America [69], and Africa [70]).

Due to the complexity and regional differences of the impact systems in plum rain season in the MLYRB, a systematic summary of the influencing systems and the characteristics of water vapor transmission and budget in this region can not only provide a scientific basis for accurately predicting of such events but also be very necessary for disastrous weather forecast and early warning.

Therefore, based on the analysis of the characteristics of the rainstorm cases in the MLYRB from 2012 to 2021, this paper studies the main impact systems, summarizes the weather circulation types, and then gives water vapor transportation and budget characteristics of different types of rainstorm cases through classification, synthesis, and water vapor tracking methods. It can help us achieve a comprehensive understanding of the weather situations and water vapor characteristics during rainstorms in plum rain season in the MLYRB and deepen our understanding on the changes and differences of precipitation characteristics under different types of weather situations. It is hoped that the research results can be used to further improve the rainstorm prediction technology and provide useful reference for disaster prevention and reduction.

2. Materials and Methods

2.1. Materials. The analysis data used for classifying and summarizing the space conceptual models of rainstorms in the MLYRB in this paper include conventional ground data, radiosonde data, and FNL (Final) Operational Global Analysis reanalysis data ($1^\circ \times 1^\circ$) from the American National Centers for Environmental Prediction and National Center for Atmospheric Research (NCEP/NCAR) from 2012 to 2021. The data used in Hybrid Single Particle Lagrangian Integrated Trajectory model (HYSPLIT 4.0) is the reanalysis data from NCEP/NCAR with temporal resolution of 6 hours and horizontal resolution of $2.5^\circ \times 2.5^\circ$, which has been packaged into an available data format (ARL) for HYSPLIT 4.0 by ARL (Air Resources Laboratory) of the National Oceanic and Atmospheric Administration (NOAA).

2.2. Study Period. The Meiyu in China is a unique rainy season during the northward advancement of the EASM in late spring and early summer. The average Meiyu period is from mid-June to mid-July, which is also the period of the strongest precipitation. The precipitation in the Meiyu period has great interannual variation. It can be continuous from several days to several weeks or intermittent, which accounts for almost half of the precipitation in the whole summer [17]. We select June to July as the main analysis period in this paper.

2.3. Study Region. The study region is located in the MLYRB (27°–34°N, 109°–123°E) (red rectangle area in Figure 1). This

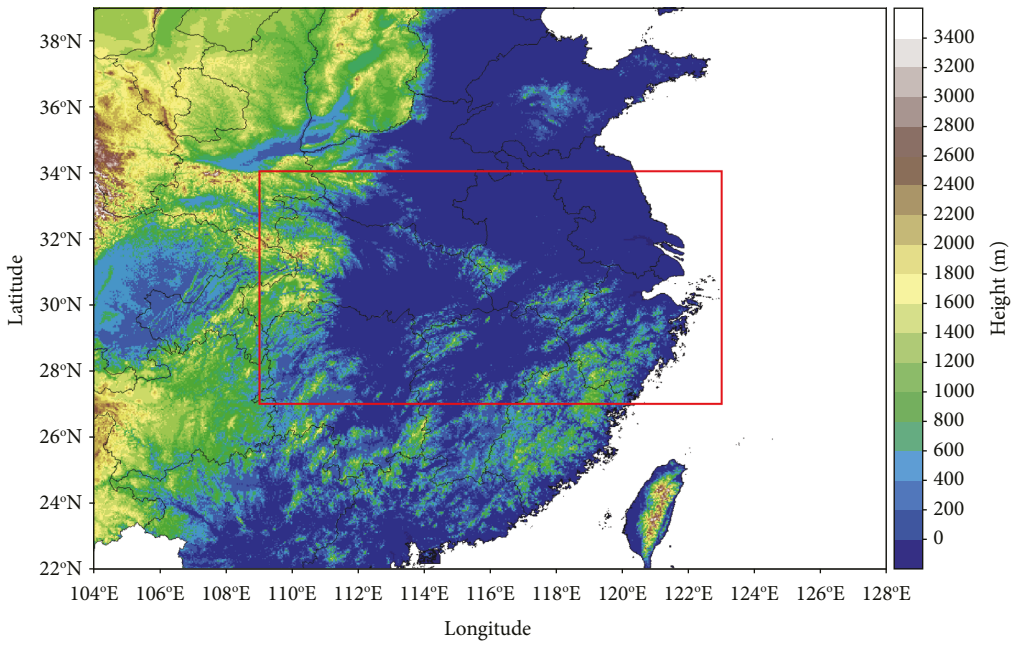

Figure 1: Study location and topography (shaded, unit: m) in the MLYRB (red rectangle area).

region is a key industrial and agricultural production base in China with continuous economic development and a high level of science, technology, and culture which encloses approximately 700,000 km^2. With high temperature and rainy season in summer and mild and little rain in winter, the climate in the MLYRB is conducive to agricultural production. At the same time, this area is one of the waterlogged areas in China. During spring and summer, especially the plum rain season from June to July, the rainfall is concentrated and heavy, which is a direct cause of water logging. With a hilly topography, sudden rainstorms produce a large amount of runoff which then pour into lakes and rivers. If there are floods upstream at the same time, this is more likely to cause flood in rivers and lakes, destroy embankments, inundate houses and farmland, and even threaten the safety of people's lives and property.

2.4. Methods

2.4.1. Classification and Synthesis Methods of Rainstorm Processes. The rainstorm cases in the MLYRB during plum rain season are analyzed from the perspective of weather types by the method of comprehensive analysis, and then the processes of the same type are synthesized. The synthetic field is the nearest reanalysis data at 00:00 UTC or 12:00 UTC before the rainstorm occurs: if the rainstorm occurs in the daytime, the reanalysis data at 00:00 UTC of the same day will be used; otherwise, the reanalysis data at 12:00 UTC of the same day will be used.

2.4.2. Introduction of Hybrid Single Particle Lagrangian Integrated Trajectory Model (HYSPLIT v4.9). Developed by the Air Resources Laboratory of NOAA, HYSPLIT v4.9 is used in this paper to provide details and changes of water vapor along the water vapor transport trajectory [71]. The initial position of tracking is selected in the MLYRB (red rectangle area in Figure 1) and the initial tracking heights chosen are 100 m, 500 m, 1500 m, 3000 m, and 5000 m, among which the levels below 1500 m are taken as the lower troposphere and the levels between 3000 m and 5000 m are taken as the middle troposphere. The model can give hourly trajectory points and 6 hourly physical fields (temperature, height, specific humidity, pseudoequivalent potential temperature, and water vapor flux) backward to 10 days by retracking every 6 hours. Although the initial heights are fixed, the height of each trajectory varies with space and time when simulated in Lagrangian space. Due to the large number of simulated trajectories, in order to see the distribution of trajectories more directly, all trajectories are clustered by merging the trajectories close to each other [71].

Based on this, we introduce the improved regional source-sink attribution method to determine the relative contribution of different sources at different levels. By calculating the change of specific humidity in the atmosphere, the contribution of each source to the precipitation in the target area can be determined quantitatively. We introduce the following formula to calculate the contribution of every channel:

$$Qs = \frac{\sum_1^m q\text{last}}{\sum_1^n q\text{last}} \times 100\%. \quad (1)$$

In the above formula, Qs represents contribution of the specific humidity or water vapor flux, $q$last represents specific humidity or water vapor at the end of the channel, m represents the number of tracks included in the channel, and n represents the total number of tracks. We can fully understand the vertical structure characteristics of water vapor contribution through this method [72–74].

2.4.3. Calculation Method of Water Vapor Budget. Consider that water vapor source is due to external evaporation and water vapor sink is due to internal condensation [75].

$$\frac{\partial q}{\partial t} + \nabla \cdot qV + \frac{\partial \omega\, q}{\partial p} = -m + E. \quad (2)$$

The above formula is the water vapor continuity equation: q is the specific humidity, V is the horizontal wind, ω is the vertical velocity, the first term on the left of the equation is the local variation of water vapor, the second term is the divergence of water vapor flux, the third term is the vertical transportation of water vapor, and M and E on the right of the equation are the condensation rate and evaporation rate, respectively. By integrating the above formula from the bottom to the top of the atmosphere and making average in the selected region, the average water vapor budget of the region can be diagnosed. If the influence of terrain and ground friction are not considered and the vertical velocity on the ground and the top of the atmosphere is considered to be 0, the third term on the left of the equation can be omitted. In the rainstorm area, the local variation of water vapor is much smaller than precipitation, so the first term on the left can also be omitted. It can be seen that the horizontal convergence of water vapor in the whole layer is approximately equal to the budget of water vapor in the region [76].

3. Results and Discussion

3.1. Weather Types and Conceptual Models of Rainstorm Processes in the MLYRB. Using synoptic diagnostic methods, 64 cases of rainstorm processes in the MLYRB during plum rain season from 2012 to 2021 are classified into 4 categories: Static Front Pattern (14 cases, SFP), Subtropical High Edge Pattern (8 cases, SHEP), Northeast Cold Vortex Pattern (15 cases, NCVP), and Low-Level Vortex and Shear Pattern (27 cases, LLVSP). Synthetic analysis is carried out in order to further explore the main weather systems, as well as dynamic, thermal, and water vapor characteristics of each type of rainstorm cases in plum rain season.

3.1.1. Static Front Pattern Rainstorms. There occurred altogether 14 SFP rainstorm cases during the 10 years. By compositing and analyzing the synoptic situations in the SFP rainstorms, it is found that the main impact systems are stably maintained Western Pacific Subtropical High (WPSH), mid-level trough, low-level shear lines, and ground stationary front. As shown in Figure 2, the circulation characteristics of SFP rainstorms are as follows.

There is a deep mid-level trough in the mid-high latitudes with strong positive vorticity advection in front of it, in spite of the small meridionality. Large-scale dynamic forcing is conducive to maintaining strong upward movement in a large area. WPSH is strong enough to control Southern China, resulting in blocking the movement of the mid-low latitude systems, which is conducive to the maintenance of heavy rainfall in the MLYRB. There are cold shear lines in lower levels which are accompanied by LLJ with moderate intensity. The heavy rainfall area of these processes is located between the cold shear line on 700 hPa and the static front, with a wide range. The distribution of the heavy rain area is similar to that of the shear lines in a northeast to southwest belt shape. The highest precipitation intensity is mainly around 50 mm/24 h. When the shear lines and strong LLJ occur at the same time, precipitation above 100 mm/24 h may also occur. Because the rain belt can last for several days or even more in the same area, rainstorms of this kind have great influences.

3.1.2. Subtropical High Edge Pattern Rainstorms. There occurred altogether 8 SHEP rainstorm cases during the 10 years. The main impact systems are stably maintained WPSH, mid-level short wave troughs, low-level shear lines, and LLJ. As shown in Figure 3, the circulation characteristics of SHEP rainstorms are as follows.

The WPSH is stably sustained in the Southeast area of China with its ridge line located near 20°N, north boundary at 25°E, and west ridge point at 100°E. Warm and humid air is transported to the MLYRB along the southwest air flow on the northwest side of the WPSH. In mid-high latitudes, there are short wave troughs developing and moving eastward continuously. Therefore, the northerly air flow behind the troughs and the southwest air flow on the north side of the WPSH converge in the MLYRB. In low levels, there occurs warm shear lines between southwest airflow and southeast airflow. Under the combined action of divergent suction of upper-level distributary area and convergence in the low levels, heavy rain forms in the MLYRB. The heavy rain locates in the south of the warm shear on 850 hPa with a quasi-east-west shape.

3.1.3. Northeast Cold Vortex Pattern Rainstorms. There occurred altogether 15 NCVP rainstorm cases during the 10 years. The main impact systems are stably maintained Northeast Cold Vortex, mid-level trough, low-level shear lines, LLJ, SLLJ, and ground cold front. As shown in Figure 4, the circulation characteristics of NCVP rainstorms are as follows.

The Northeast Cold Vortex is established and remains in the Northeastern China with its central intensity reaching 5360 gpm. While the intensity of the Northeast Cold Vortex continues to strengthen because of continuous supplement of cold air from the west side of Baikal Lake, the ridge in the north of Okhotsk Sea also develops, which prevents the Northeast Cold Vortex from moving eastward. At the same time, the WPSH continues to extend westward and northward to South China, which brings rich water vapor and unstable energy to the MLYRB along the LLJ and SLLJ in the northeast of WPSH. The strong convergence of warm air from the edge of the WPSH and cold air from the Northeast Cold Vortex occurs in the MLYRB, resulting in heavy rain processes with the characteristics of strong intensity and coexistence of multiple disasters. During this type of rainstorms, the high- and low-level jets remain on 200 hPa, 850 hPa, 700 hPa, and 925 hPa, the Northeast Cold Vortex is strong and stable, the WPSH is in a northeast to southwest

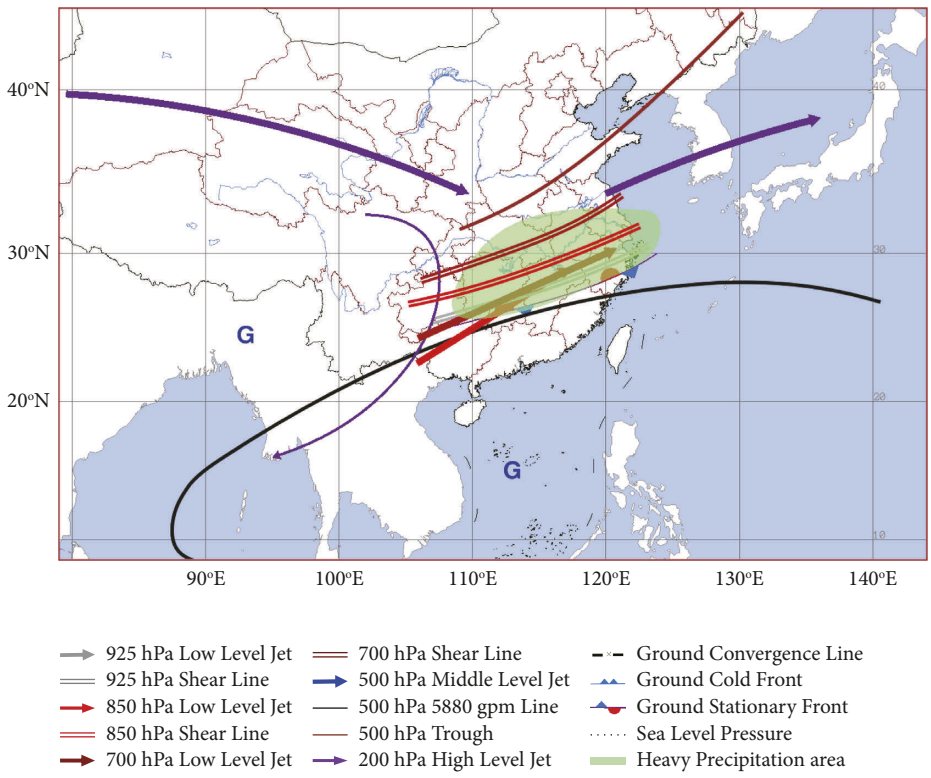

Figure 2: Conceptual model of the static front pattern rainstorms.

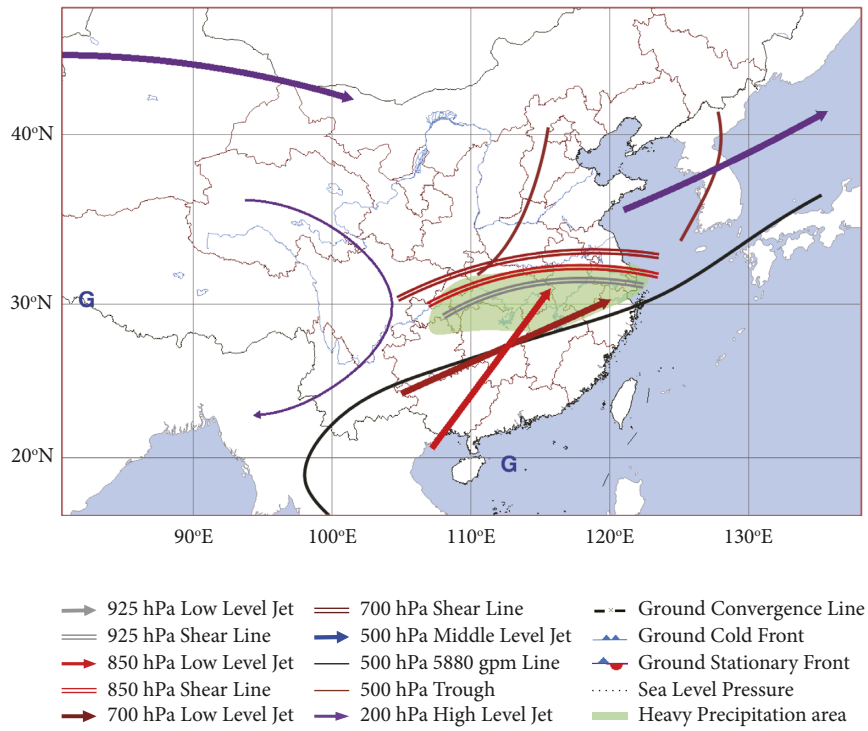

Figure 3: Conceptual model of the subtropical high edge pattern rainstorms.

belt, and the trough is in a large meridional direction. Such kind of precipitation has mobility characteristics, which is well coordinated with the shape of the Northeast Cold Vortex and low-level shear lines.

3.1.4. Low-Level Vortex and Shear Pattern Rainstorms. There occurred altogether 27 LLVSP rainstorm cases during the 10 years. The main impact systems are mid-level trough, low-level vortexes, shear lines, LLJ, SLLJ, and ground

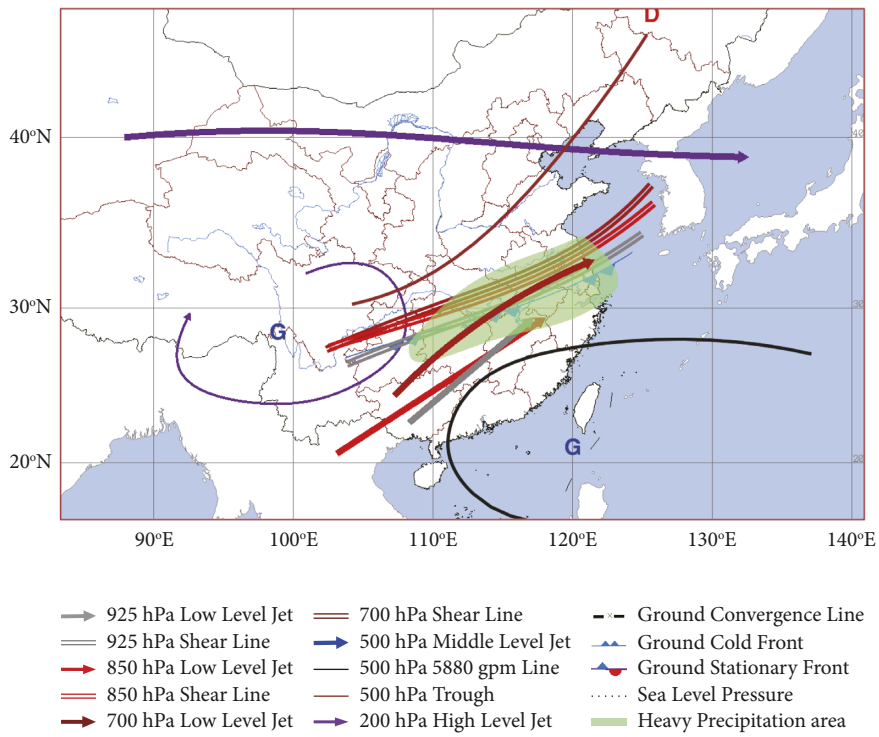

Figure 4: Conceptual model of the Northeast Cold Vortex pattern rainstorms.

inverted trough. As shown in Figure 5, the circulation characteristics of LLVSP rainstorms are as follows.

There is a mid-level trough occurring in mid-high latitudes with large meridionality. Under the action of positive vorticity advection in front of the trough, a low-level vortex generates and moves eastward with strong LLJ and SLLJ in front of it. The WPSH in this type is relatively weak and located on sea. Located between the trough and the WPSH, the MLYRB is under the influence of strong warm and humid southwest airflow and warm inverted trough extending from the southwest to the northeast, providing favorable thermal and dynamic environment conditions for the generation of small- and medium-scale disturbances. Heavy rainfall occurs in the southeast of the vortex, the south of the warm shear lines, and the east of the cold shear lines. Frequently, it also occurs in the outlet of the LLJ and SLLJ in the warm air region [77, 78]. The distribution of rain belt is consistent with the shape of the vortex with the maximum intensity exceeding 100 mm/24 h, which is prone to extremely heavy rain magnitude precipitation (250 mm/24 h). Therefore, when faced with the LLVSP rainstorms, forecasters should pay attention to the configuration of the shear lines and the LLJ in addition to the generation and disappearance of the low vortex and its moving path.

3.2. Water Vapor Trajectory Analysis. Since water vapor locates mainly below 500 hPa, the temporal and spatial evolution of water vapor in lower and middle levels are analyzed. The water vapor transport characteristics in each type of rainstorms are analyzed using clustered backward trajectories.

There are four main water vapor transport channels in the lower layers of the STP rainstorms according to Figure 6(a). The most important channel is from the South China Sea (accounts for 51.47% of the total number of low-level trajectories, and the contribution rates of specific humidity and water vapor flux are about 53%). The second one is from the Bay of Bengal (accounts for 23.13% and the contribution rates of specific humidity and water vapor flux are about 24% (Table 1)) and it enters into the MLYRB through the Indochina Peninsula. The third one is from the Yellow Sea, followed by the high latitude inland channel, which indicates the cold air from West Siberia. There are also four main water vapor transport channels in the lower layers of the SHEP rainstorms (Figure 6(c)). The main channel is from the Bay of Bengal (accounts for 40.73% and the contribution of specific humidity and water vapor flux is about 38% (Table 1)), followed by the channel from the Bay of Bengal-South China Sea, the Yungui Plateau, and the west Pacific Ocean. The channel from the Yungui Plateau is the shortest, which indicates the slow motion of water vapor in this channel. In the lower layers of the NCVP rainstorms (Figure 6(e)), the main channel is from Bohai (accounts for 38.17% and the contribution of specific humidity and water vapor flux is about 34% (Table 1)) and it enters into the MLYRB through the Shandong Peninsula. It is followed by the Bay of Bengal channel, the Bay of Bengal-South China Sea channel, and the South China Sea channel. In the lower layers of the LLVSP rainstorms (Figure 6(g)), the main channel is from the Bay of Bengal (accounts for 28.9% and the contribution of specific humidity and water vapor flux is about 28% (Table 1)), followed by the Bay of Bengal-South China Sea channel, the Yellow Sea channel, and the South China Sea channel.

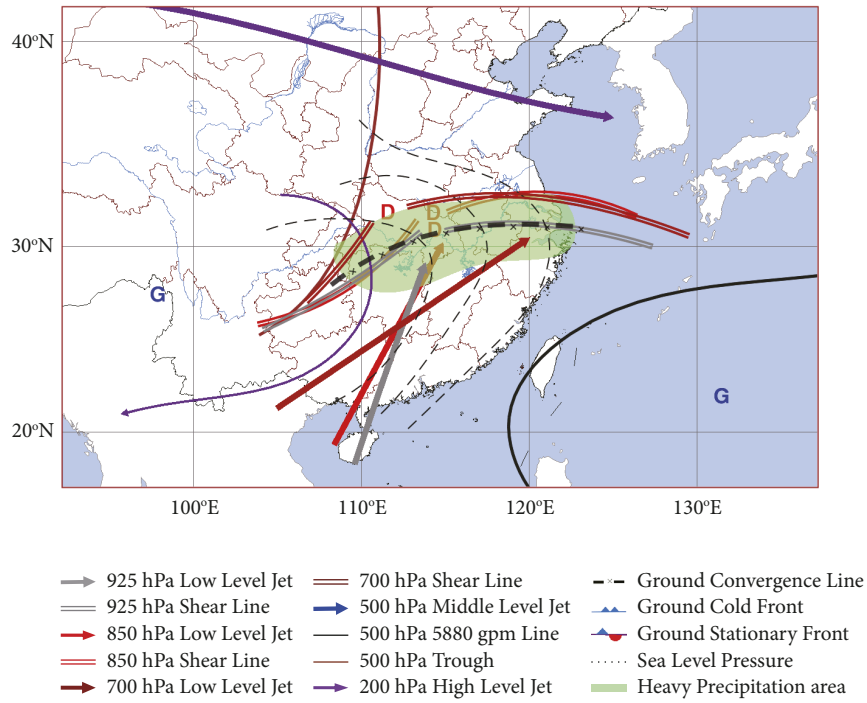

Figure 5: Conceptual model of the Low-Level Vortex and Shear Pattern rainstorms.

It can be seen from the height evolution of the lower-level water vapor channels that, in the SFP rainstorms (Figure 6(b)), channels 1 and 2 coming from the ocean surface in low latitude with height between 940 hPa and 900 hPa are slightly elevated due to the topographic force of Nanling Mountain after landing. Channel 6 is the shortest, indicating that the air mass in this channel moves slowly and is slightly elevated through the hilly area of Shandong Province. All the 3 channels are transported to the height around 900 hPa in MLYRB. Channel 7 coming from the high latitude inland with the initial height around 650 hPa sinks into the MLYRB in form of cold air, which strengthens the atmospheric baroclinity. The long track of channel 7 indicates the fast movement of dry and cold air.

In the SHEP rainstorms (Figure 6(d)), channels 1, 3, and 4 all come from ocean surface. Due to the obvious elevation of Nanling Mountain and Luoxiao Mountain, the water vapor of channel 1 is finally transported to the MLYRB around 850 hPa, while water vapor of channel 3 and that of channel 4 are also elevated slightly by the Nanling Mountains and finally transported to the MLYRB near 920 hPa and 940 hPa, respectively. The water vapor of channel 8 moves slowly across the Qinling Mountain, so it rises earlier and sinks later to around 880 hPa.

Channels 1, 2, and 4 of the NCVP rainstorms (Figure 6(f)) coming from ocean surface in low latitude move quickly through the Yungui Plateau and the Nanling Mountain with height elevated obviously and finally are transported to the vicinity of 900 hPa (for channels 2 and 4) and 860 hPa (for channel 1) in the MLYRB. The water vapor of channel 5 from Bohai is also elevated to a higher altitude during passing through the hilly area of Shandong and transported to the MLYRB near 900 hPa.

The water vapor channels 1, 2, and 4 of the LLVSP rainstorms (Figure 6(h)) which are similar to those of the NCVP are finally transported to the height between 920 hPa and 850 hPa in the MLYRB. Channel 6 coming from the Yellow Sea is lifted obviously to around 900 hPa after passing through the Yangtze River Delta and the Dabie Mountain.

According to the previous analysis, it can be seen that the water vapor channels in lower levels and lower latitude regions account for the majority, while the air mass from the north in higher latitude has little influence. So we further explore the distribution of water vapor channels in middle layers.

There are four main water vapor transport channels in the middle layers of the STP rainstorms according to Figure 7(a). The most important channel is from the Bay of Bengal, which accounts for 43.65% of the total number of the middle-level trajectories, and the contribution rates of specific humidity and water vapor flux are about 50% (Table 2). It is followed by the South China Sea channel, the high latitude inland channel, and the Hetao channel. The high latitude inland channel and the Hetao channel indicate the cold air from the north. In the middle layers of the SHEP rainstorms (Figure 7(c)), the main channel remains that from the Bay of Bengal with trajectories accounting for 62.95% of the total number of the middle-level trajectories and the contribution of specific humidity and water vapor flux being about 70% (Table 2), which indicates the transportation of large amount of water vapor through the southwest air flow on the edge of the WPSH. It is followed by the Indo-China Peninsula channel, the Bay of Bengal-South China Sea channel, and the high latitude inland channel. In the middle layers of the NCVP rainstorms (Figure 7(e)), the main channel remains that from the Bay of Bengal (accounts

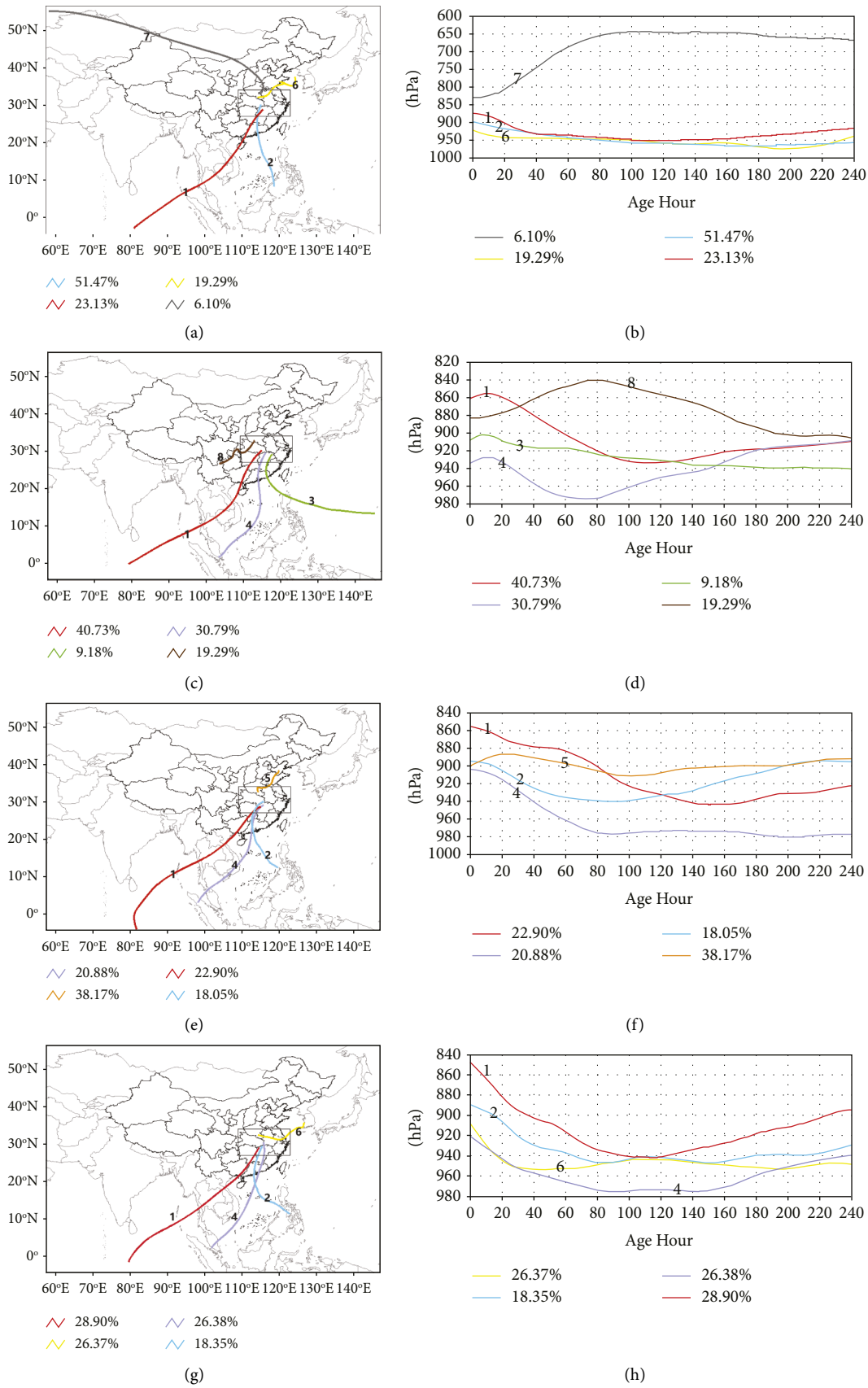

Figure 6: The spatial distribution of lower-level water vapor channels (a, c, e, g) and their height evolution (b, d, f, h) ((a, b) for SFP, (c, d) for SHEP, (e, f) for NCVP, and (g, h) for LLVSP).

Table 1: The total number of trajectories and contribution of specific humidity and water vapor flux on the lower levels of different types of rainstorms.

Rainstorm types	Physical quantities	Bay of Bengal channel (1)	South China Sea channel (2)	Western Pacific-South China Sea channel (3)	Bay of Bengal-South China Sea channel (4)	Bohai channel (5)	Yellow Sea channel (6)	High latitude inland channel (7)	Yungui Plateau channel (8)
SFP	Total trajectories	1804	4015				1505	476	
	Contribution of specific humidity (%)	24.78	53.54				18.63	3.02	
	Contribution of water vapor flux (%)	24.80	53.57				18.60	2.98	
SHEP	Total trajectories	3177		716	2402				1505
	Contribution of specific humidity (%)	38.52		9.22	34.84				17.41
	Contribution of water vapor flux (%)	38.46		9.22	34.94				17.38
NCVP	Total trajectories	1786	1408		1629	2977			
	Contribution of specific humidity (%)	23.41	18.49		23.33	34.77			
	Contribution of water vapor flux (%)	23.42	18.49		23.38	34.71			
LLVSP	Total trajectories	2254	1431		2058		2057		
	Contribution of specific humidity (%)	28.36	17.10		28.82		25.72		
	Contribution of water vapor flux (%)	28.33	17.08		28.86		25.72		

for 56.01% and the contribution of specific humidity and water vapor flux is about 62% (Table 2)). It is followed by the Southwest China channel with a slow moving speed, the Somali jet channel, and the high latitude inland channel. In the middle layers of the LLVSP rainstorms (Figure 7(g)), the main channel remains that from the Bay of Bengal (accounts for 49.62% and the contribution of specific humidity and water vapor flux is about 52% (Table 2)). It is followed by the Somali jet channel, the high latitude inland channel, and the Yangtze River Delta channel.

It can be seen that the main water vapor channel in middle layers is from the Bay of Bengal with the contribution rates of specific humidity and water vapor flux more than half (Table 2), which indicates the continuous transportation of water vapor from the Bay of Bengal to the MLYRB through the southwest jet stream and sufficient water vapor conditions for the occurrence of heavy rain in the MLYRB.

It can be seen from the height evolution of middle-level water vapor channels that, in the SFP rainstorms (Figure 7(b)), channels 1 and 2 coming from ocean surface in low latitude with track height around 950 hPa are obviously elevated due to the quick movement through topographic area. Channels 6 and 7 coming from the high latitude inland with a high initial height sink to the vicinity of 700 hPa in the MLYRB finally.

In the SHEP rainstorms (Figure 7(d)), channels 1, 3, and 5 coming from ocean surface with initial height below 800 hPa are finally transported to the MLYRB around 700 hPa, while water vapor of channel 7 from the high latitude inland with initial height around 550 hPa is finally transported to the MLYRB in the form of cold air.

The water vapor in channels 1 and 4 of the NCVP rainstorms (Figure 7(f)) coming from ocean surface in the low latitude moves quickly through the mountain areas with height elevated obviously and is transported to the vicinity of 700 hPa in the MLYRB. The water vapor of channel 7 from the high latitude inland with initial height around 600 hPa is finally transported to the MLYRB in the form of cold air. The water vapor of channel 8 from Southwest China is slightly elevated to a higher altitude due to the slow motion when passing through hilly areas. Both channels 7 and 8 are transported to the vicinity of 700 hPa in the MLYRB.

The water vapor in channels 1 and 4 of the LLVSP rainstorms (Figure 7(h)) which is similar to that of the NCVP rainstorms is finally transported to the vicinity of 700 hPa in the MLYRB. Channel 7 coming from the high

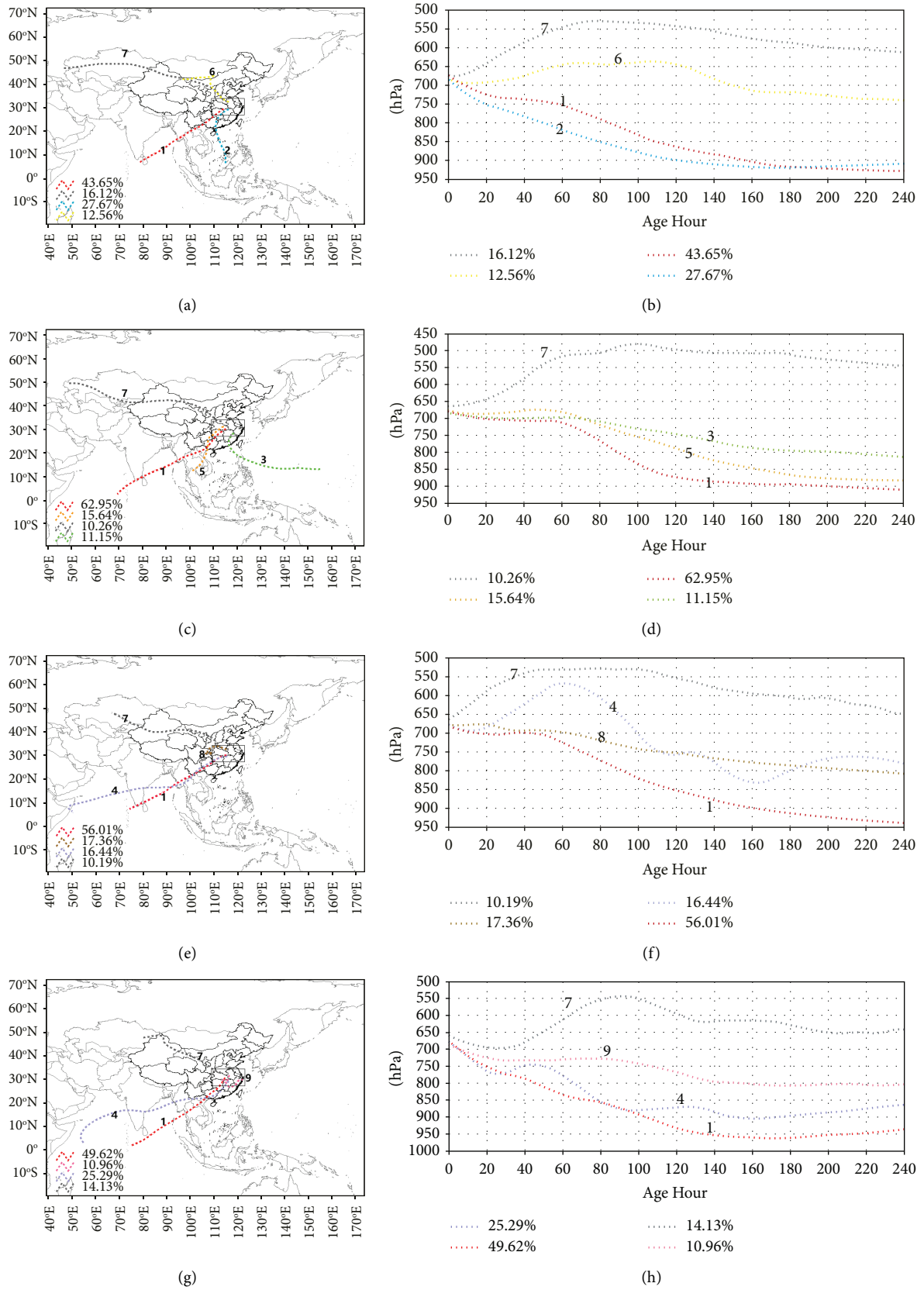

Figure 7: The spatial distribution of middle-level water vapor channels (a, c, e, g) and their height evolution (b, d, f, h) ((a, b) for SFP, (c, d) for SHEP, (e, f) for NCVP, and (g, h) for LLVSP).

Table 2: The total number of trajectories and contribution of specific humidity and water vapor flux on the middle levels of different types of rainstorms.

Rainstorm types	Physical quantities	Bay of Bengal channel (1)	South China Sea channel (2)	Western Pacific-South China Sea channel (3)	Somali jet channel (4)	Indochinese Peninsula channel (5)	Hetao channel (6)	High latitude inland channel (7)	Southwest China inland channel (8)	Yangtze River Delta channel (9)
SFP	Total trajectories	1135	720				326	419		
	Contribution of specific humidity (%)	50.52	29.33				10.23	9.92		
	Contribution of water vapor flux (%)	50.60	29.34				10.19	9.87		
SHEP	Total trajectories	1637		290		407		266		
	Contribution of specific humidity (%)	70.08		9.39		14.39		6.14		
	Contribution of water vapor flux (%)	70.16		9.37		14.37		6.10		
NCVP	Total trajectories	1456			427			265	452	
	Contribution of specific humidity (%)	62.72			16.12			6.48	14.68	
	Contribution of water vapor flux (%)	62.79			16.10			6.46	14.65	
LLVSP	Total trajectories	1290			658			367		285
	Contribution of specific humidity (%)	52.05			28.44			10.33		9.19
	Contribution of water vapor flux (%)	52.08			28.48			10.28		9.16

latitude inland with initial height near 600 hPa sinks and invades the MLYRB in the form of cold air. Channel 9 coming from the Yangtze River Delta is lifted slowly to around 700 hPa in the MLYRB under the influence of Dabie Mountain.

3.3. Water Vapor Budget Analysis. In order to analyze the water vapor transportation and budget during the four different types of rainstorms, the boundary water vapor flux and regional water vapor revenue and expenditure in the MLYRB during the rainstorm period are calculated as follows.

It can be seen from the vertical integrated water vapor flux at the boundaries of MLYRB that there are same characteristics in the four types of rainstorm cases (Figure 8): Firstly, the south boundary of the MLYRB is the most important water vapor input boundary, followed by the west boundary, while the east and north boundaries are the outflow boundaries. From the above trajectory analysis in Section 3.2, it can be seen that water vapor mainly flows into the rainstorm area through Southwest and Southern China. Secondly, there is obvious positive water vapor income in the MLYRB, which means that the MLYRB is the water vapor convergence area. We can see from the water vapor flux at the south and west boundaries that the water vapor input at different boundaries is determined by the difference of the moisture channels and the strength of LLJ.

In the NCVP (Figure 8(c)) and LLVSP (Figure 8(d)) rainstorm cases, the position of the WPSH is eastward, and the positive vorticity advection in front of the mid-level troughs with large meridionality is strong. The strong potential gradient between the mid-level troughs and the WPSH strengthens the LLJ and SLLJ, too. Therefore, the water vapor flux at the south boundary of the above two types (especially in the LLVSP) of rainstorms is the strongest. At the north boundary, there are relatively strong outputs in the SHEP (Figure 8(b)) and the LLVSP

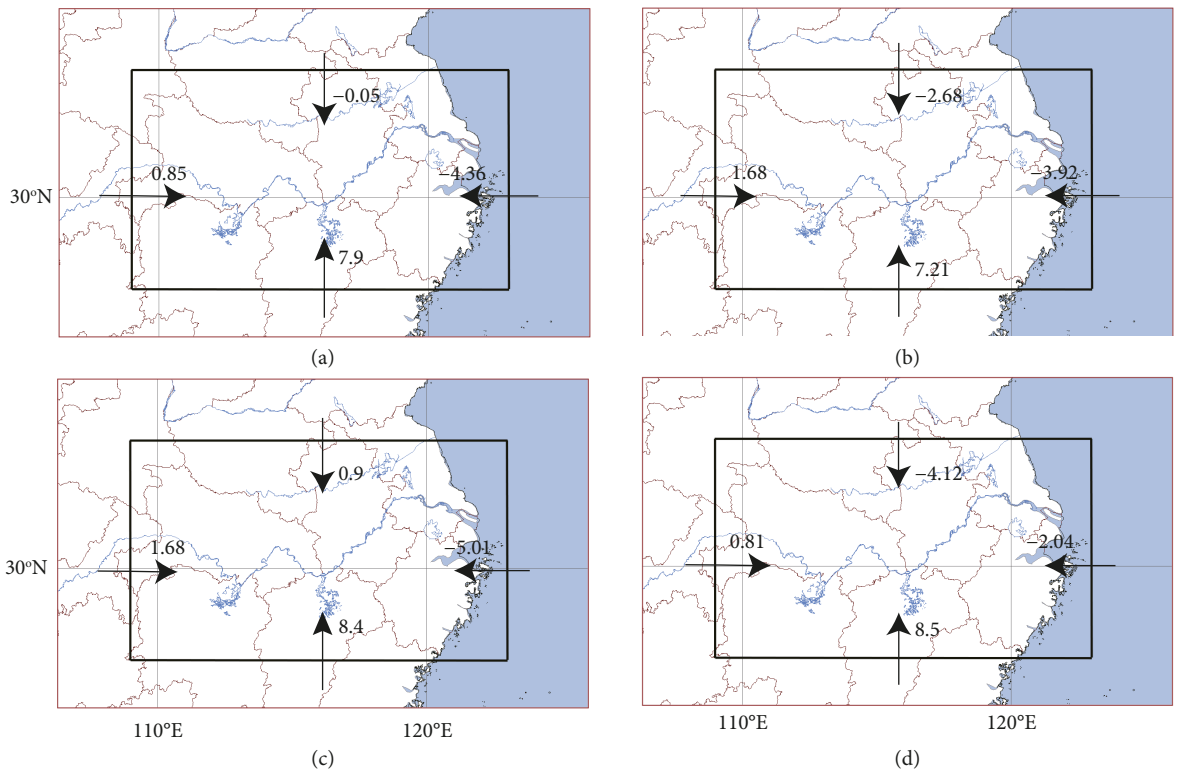

Figure 8: The average vertical integrated water vapor flux on the boundaries of the 4 types of rainstorm cases (unit: 10^7 kg/s). (a) SFP, (b) SHEP, (c) NCVP, and (d) LLVSP.

(Figure 8(d)) rainstorm cases, while there is a weak output in the SFP (Figure 8(a)) rainstorms and weak input in the NCVP rainstorms. Because of the obvious cold air activity in the NCVP and the SFP rainstorm cases, there is obvious northerly wind flow in either lower or middle layers, which makes the integral water vapor transport positive in the north boundary.

From the perspective of total regional water vapor income, the largest net water vapor income occurs in the NCVP and SFP rainstorm cases, resulting in short-duration heavy rain and strong convective weather with the accompaniment of the strong convergence of cold and warm air. However, because of the obvious mobility character in the NCVP rainstorms, the 24-hour accumulated precipitation is not the largest.

It can be seen from the vertical distribution of the averaged water vapor flux of the four types of rainstorms (Figure 9) before rainstorms occur that there is obvious outflow at the east boundary except in the low levels of the LLVSP rainstorms (strong inflow), while there is inflow in all levels above 850 hPa at the west boundary in all the four types. The water vapor transportation centers at the east and south boundaries are below 800 hPa, which are mainly coordinated with LLJ and SLLJ. The water vapor transportation at the south boundary is generally the same as the center located around 850 hPa, while there are obvious differences at the north boundary. At the north boundary, there is obvious outflow on lower layers and weak inflow on middle layers of the SHEP and LLVSP rainstorms, while there is obvious inflow on both middle and lower layers of the NCVP rainstorms. There are weak transportation centers \in the middle troposphere (around 600–500 hPa) at the north boundary, indicating that the four types of rainstorm cases are accompanied by the invasion of weak cold air on middle layers, especially in the NCVP rainstorms. From the vertical distribution of the water vapor budget, we can see that the SHEP and the NCVP rainstorm cases have the strongest water vapor flux convergence of the low levels and are more likely to produce strong short-term rainstorms.

3.4. Discussion. The study of weather system classification is helpful for forecasters to identify the weather situations and their configuration relationship with heavy rain in the MLYRB and judge the possibility of heavy rain, which is essential for the prediction of heavy rain in plum rain season. However, the classification is based on the synoptic scale systems, while the direct producers of rainstorms are usually the small- and medium-scale systems [34, 79, 80]. There exists obvious convective character with 6-hour precipitation more than 160 mm in the NCVP and SHEP rainstorms, while it is a little weaker in the other two types (figure omitted). We can also see Mesoscale Convective Complex (MCC) and Mesoscale Convective Systems (MCSs) [16, 28, 81, 82] which are the main cause of convective precipitation embedded in the large-scale precipitation cloud systems (Figure omitted). It means that there exists mesoscale weather systems in the process of Meiyu events. The stable maintenance of planetary scale systems such as

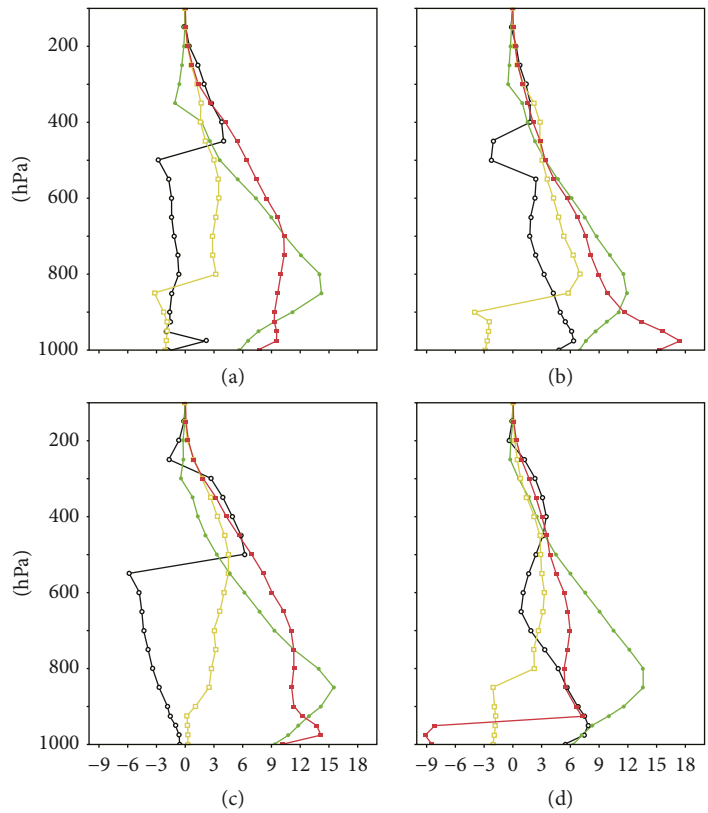

Figure 9: Vertical distribution of averaged water vapor flux from the east boundary (red line), south boundary (green line), west boundary (yellow line), and north boundary (black line) during the SFP (a), SHEP (b), NCVP (c) LLSVSP and (d) rainstorm cases (unit: $g \cdot cm^{-1} \cdot hPa^{-1} \cdot s^{-1}$).

the WPSH and the South Asia High makes the rain belt remain in the MLYRB. The synoptic systems such as shear lines, LLJ, SLLJ, low vertexes, and fronts make the environment suitable for convective systems. Convergence of dry and cold airflow with warm and wet airflow from the ground to the middle troposphere and upward movement along the Meiyu front increase the instability and stimulate the release of large amount of unstable energy [29]. Therefore, in the operational forecasting, forecasters should analyze the environmental conditions, structural characteristics, and evolution of the small- and medium-scale systems on the basis of the large scale weather classification, make accurate forecast of the possible falling area, intensity, and starting and ending time of rainstorms, and release the early warning signal in the nowcasting stage with the help of the numerical forecast and observation data.

4. Conclusions

Based on conventional observation data and reanalysis data from NCEP/NCAR between 2012 and 2021, combined with the meteorological analysis, composite synthesis, and water vapor trajectory analysis, the weather circulations of typical rainstorms during the 10 years can be divided into 4 categories: Static Front Pattern (14 cases, SFP), Subtropical High Edge Pattern (8 cases, SHEP), Northeast Cold Vortex Pattern (15 cases, NCVP), and Low-Level Vortex and Shear Pattern (27 cases, LLVSP).

The SHEP and SFP rainstorm cases have the characteristics of long duration and wide range, while the NCVP rainstorms are characterized by mobility and disaster weather accompaniment. The LLVSP rainstorms are accompanied by strong low-level jet (LLJ) and super low-level jet (SLLJ), so the daily precipitation of this type has extremity feature. Most of the rainstorms are accompanied by high-level jet and low-level jet, indicating the obvious coupling effect of high-level and low-level systems in the rainstorm cases during plum rain season. The occurrence and development of rainstorms are all well coordinated with the systems on lower levels.

By analyzing the characteristics of water vapor transport in lower layers (below 1500 m) and middle layers (3000 m–5000 m) during the four types of rainstorms, the vertical structure of water vapor transport is obtained. The main water vapor channel in the lower layers of the SFP is from the South China Sea, while it is from Bohai for the NCVP rainstorms and the Bay of Bengal for the SHEP and LLVSP rainstorms. The main water vapor channel in middle layers is from the Bay of Bengal with contribution rate accounting for 62.95% in the SHEP, followed by NCVP (56.01%), the LLVSP (49.26%), and the SFP (43.65%) because of the affection of the southwest air flow.

The south boundary of the MLYRB is the most important water vapor input boundary, followed by the west boundary, while the east and north boundaries are the outflow boundaries. During the rainstorm cases, the low-

level water vapor is exuberant, and the low-level water vapor convergence is stronger than the high-level divergence. Among the four types of rainstorms, the NCVP rainstorms provide the most abundant low-level water vapor convergence, resulting in the strongest short-term precipitation intensity among the four types. Combined with water vapor transportation and convergence, the refined spatial conceptual models of the four types of rainstorms can better judge the process intensity and falling area and provide reference for disastrous weather forecast and early warning.

Data Availability

The Grid data used in this study are obtained from https://rda.ucar.edu/datasets/ds083.2/index.html and ftp://arlftp.arlhq.noaa.gov/pub/archives/reanalysis. The rainstorm cases used in this paper are from the rainstorm case datasets of the China Meteorological Administration.

Conflicts of Interest

The authors declare that they have no conflicts of interest.

Acknowledgments

Financial support for this study was provided by the Key Projects of Shandong Meteorological Bureau (2020SDQXZ02), the Major Basic Research Project of Natural Science Foundation of Shandong Province (ZR2019ZD12), the Special Project of Hunan Meteorological Bureau (XQKJ21C010), and the Key Innovation Team of the China Meteorological Administration (CMA2022ZD04).

References

[1] S. Y. Tao, "The relationship between Meiyu in far east and the behaviour of circulation over Asia," *Acta Meteorologica Sinica*, vol. 29, pp. 119–134, 1958.

[2] D. Ye, S. Y. Tao, and M. Li, "The abrupt change of circulation over northern hemisphere during June and octorber," *Acta Meteorologica Sinica*, vol. 29, pp. 249–263, 1958.

[3] S. Y. Tao and L. X. Chen, "A review of recent research on the east Asia summer monsoon in China," *Monsoon Meteorology*, pp. 60–92, 1987.

[4] Y. H. Ding, "Summer monsoon rainfalls in China," *Journal of the Meteorological Society of Japan. Ser. II*, vol. 70, no. 1B, pp. 373–396, 1992.

[5] L. Li and Y. Zhang, "Effects of different configurations of the east Asian subtropical and polar front jets on precipitation during the mei-yu season," *Journal of Climate*, vol. 27, no. 17, pp. 6660–6672, 2014.

[6] H. Li, S. He, K. Fan, and H. Wang, "Relationship between the onset date of the Meiyu and the south Asian anticyclone in April and the related mechanisms," *Climate Dynamics*, vol. 52, no. 1-2, pp. 209–226, 2019.

[7] H. Li, S. He, K. Fan, Y. Liu, and X. Yuan, "Recent intensified influence of the winter north pacific Sea surface temperature on the Meiyu withdrawal date," *Journal of Climate*, vol. 34, no. 10, pp. 3869–3887, 2021.

[8] Y. Yuan, H. Gao, and W. J. Li, "Analysis and comparison of summer precipitation features and physical mechanisms between 2016 and 1998," *Acta Meteorologica Sinica*, vol. 75, no. 1, pp. 19–38, 2017.

[9] Y. H. Ding, P. Liang, Y. J. Liu, and Y. C. Zhang, "Multiscale variability of Meiyu and its prediction: a new review," *Journal of Geophysical Research: Atmospheres*, vol. 125, no. 7, Article ID e2019JD031496, 2020.

[10] Z. Q. Zhou, S. P. Xie, and R. H. Zhang, "Historic Yangtze flooding of 2020 tied to extreme Indian Ocean conditions," *Proceedings of the National Academy of Sciences of the United States of America*, vol. 118, no. 12, Article ID e2022255118, 2021.

[11] H. Li, B. Sun, H. J. Wang, and X. Yuan, "Joint effects of three oceans on the 2020 super Meiyu," *Atmospheric and oceanic science letters*, vol. 15, pp. 100127–100129, 2022.

[12] Q. Y. Zhang and S. Y. Tao, "Influence of Asian mid-high latitude circulation on East Asian summer rainfall," *Acta Meteorologica Sinica*, vol. 56, no. 2, pp. 199–211, 1998.

[13] Q. Y. Zhang and H. Guo, "Circulation differences in anomalous rainfall over the Yangtze river and Huaihe river valleys in summer," *Chinese Journal of Atmospheric Sciences*, vol. 38, no. 4, pp. 656–669, 2014.

[14] Z. G. Feng, X. W. Cheng, X. Chen, and A. Q. Nie, "The classification of the circulations and the climatic characteristics of rainstorms in Huaihe river basin," *Journal of Tropical Meteorology*, vol. 29, no. 5, pp. 824–832, 2013.

[15] R. H. Jin, M. Y. Jiao, J. Xu, and H. F. Qin, "Abnormal characteristics and causes analysis of the western pacific subtropical high activity during the Huaihe floods in 2003," *Journal of Tropical Meteorology*, vol. 22, no. 1, pp. 60–66, 2006.

[16] D. Si, Y. H. Ding, and Y. J. Liu, "Decadal northward shift of the Meiyu belt and the possible cause," *Science Bulletin*, vol. 54, no. 24, pp. 4742–4748, 2009.

[17] Y. H. Ding, J. J. Liu, Y. Sun, Y. J. Liu, J. H. He, and Y. F. Song, "A study of the synoptic-climatology of the Meiyu system in east Asia," *Chinese Journal of Atmospheric Sciences*, vol. 31, no. 6, pp. 1082–1101, 2007.

[18] P. Liang, X. Tang, X. X. Ke, and J. H. He, "Review of study on influencing factors of China Meiyu," *Scientia Meteorologica Sinica*, vol. 27, no. 4, pp. 464–471, 2007.

[19] N. F. Zhou, Y. Li, and X. L. Jia, "Relationship between heavy precipitation and atmospheric wave with different time scales during Meiyu period in Yangtze-Huai River region," *Journal of Tropical Meteorology*, vol. 37, no. 1, pp. 14–24, 2021.

[20] J. H. Sun, J. Wei, S. X. Zhao, and S. Y. Tao, "The abnormal weather and its circulation in summer of 2009," *Journal of Meteorological Research*, vol. 16, no. 2, pp. 209–220, 2011.

[21] R. Y. Niu and B. Zhou, "Analysis of abnormal characteristics and causes of Meiyu Overthe Yangtze-Huaihe river basin in 2019," *Meteorological Monthly*, vol. 47, no. 11, pp. 1347–1358, 2021.

[22] Q. Gao and X. P. Yao, "Evolution characteristics and effect on precipitation of dry cold air in the middle and lower reaches of the Yangtze river during 2020 Meiyu period," *Torrential Rain and Disasters*, vol. 40, no. 4, pp. 342–351, 2021.

[23] X. Su, Z. M. Kang, and X. R. Zhuang, "Uncertainty analysis of heavy rain belt forecast during 2020 Meiyu period," *Meteorological Monthly*, vol. 47, no. 11, pp. 1336–1346, 2021.

[24] S. P. Sun, G. L. Feng, Z. H. Zhang, J. Xie, and J. H. Zhao, "Study on the stable components of atmospheric circulation during the continuous heavy rainfall of Meiyu in 2016," *Chinese Journal of Atmospheric Sciences*, vol. 45, no. 2, pp. 245–256, 2021.

[25] J. J. Wang and S. Y. Tao, "Structure and formation of Meiyu front in 1998," *Journal of Applied Meteorology and Climatology*, vol. 13, no. 5, pp. 526–534, 2002.

[26] D. C. Ye, Z. H. Guan, and S. Y. Sun, "The relationship between heavy precipitation in the middle and lower reaches of Yangtze river and baroclinic wave packets in the upper troposphere during the Meiyu period of 2016," *Acta Meteorologica Sinica*, vol. 77, no. 1, pp. 73–83, 2019.

[27] Y. H. Ding, Y. Y. Liu, and Z. Z. Hu, "The record-breaking Meiyu in 2020 and associated atmospheric circulation and tropical SST anomalies," *Advances in Atmospheric Sciences*, vol. 38, no. 12, pp. 1980–1993, 2021.

[28] S. L. Zhang, S. Y. Tao, Q. Y. Zhang, and J. Wei, "Large and meso-α scale characteristics of intense rainfall in the mid-and lower reaches of the Yangtze Rive," *Chinese Science Bulletin*, vol. 47, no. 9, pp. 779–786, 2002.

[29] T. Akiyama, "A medium-scale cloud cluster in a Baiu front: part I: evolution process and fine structure," *Journal of the Meteorological Society of Japan. Ser. II*, vol. 62, no. 3, pp. 485–504, 1984.

[30] R. H. Huang, D. Chen, and Y. Liu, "Characteristics and causes of the occurrence of flooding disaster and persistent heavy rainfall in the Yangtze river valley of China," *Journal of Chengdu University of Technology*, vol. 27, no. 1, pp. 1–19, 2012.

[31] X. F. Wang, X. K. Wang, and G. R. Xu, "Analysis on environment of meso-β-scale system of continuous heavy rainstorm over the middle reach of Yangtze river durin Meiyu period in 2010," *Plateau Meteorology*, vol. 32, no. 3, pp. 750–761, 2013.

[32] Y. Y. Bao, "Similarities and differences of monsoon circulations between 2016 and 1998 Meiyu periods in the middle and lower reaches of the Yangtze river and the comparison of their physical mechanisms," *Chinese Journal of Atmospheric Sciences*, vol. 45, no. 5, pp. 994–1006, 2021.

[33] J. H. Zhao, H. Zhang, J. Q. Zuo, K. G. Zuo, and L. J. Chen, "What drives the super strong precipitation over the Yangtze–Huaihe river basin in the Meiyu period of 2020?" *Chinese Journal of Atmospheric Sciences*, vol. 45, no. 6, pp. 1433–1450, 2021.

[34] Y. L. Luo and Y. R. X. Chen, "Investigation of the predictability and physical mechanisms of an extreme-rainfall-producing mesoscale convective system along the Meiyu front in east China: an ensemble approach," *Journal of Geophysical Research-atmospheres*, vol. 120, no. 20, pp. 10593–10618, 2015.

[35] Y. M. Yang, W. L. Gu, R. L. Zhao, and J. Liu, "The statistical analysis of low vortex during Meiyu season in the lower reaches of the Yangtze," *Journal of Applied Meteorology and Climatology*, vol. 21, no. 1, pp. 11–18, 2010.

[36] J. Y. Liu, Z. M. Tan, and Y. Zhang, "Study of the three types of torrential rains of different formation mechanism during the Meiyu period," *Acta Meteorologica Sinica*, vol. 70, no. 3, pp. 452–466, 2012.

[37] S. Y. Tao, *The Torrential Rain in China*, Science Press, Beijing, China, 1980.

[38] R. A. Maddox, C. F. Chappell, and L. R. Hoxit, "Synoptic and meso-α scale aspects of flash flood events 1," *Bulletin of the American Meteorological Society*, vol. 60, no. 2, pp. 115–123, 1979.

[39] J. J. Chen, C. Z. Ye, and X. Y. Wu, "Objectively classified patterns of atmospheric circulation for rainstorm events in flood season in Hunan," *Torrential Rain and Disasters*, vol. 35, no. 2, pp. 119–125, 2016.

[40] Q. H. Deng and J. Y. Zhang, "Cloud cluster concept models for nowcasting regional disastrous heavy rain," *Journal of Nanjing Institute of Meteorology*, vol. 13, no. 4, pp. 561–567, 1990.

[41] Y. G. Zheng, J. Chen, and G. Q. Ge, "Review on the synoptic scale Meiyu front system and its synoptics definition," *Acta Scientiarum Nauralium Universitaties Pekinensis*, vol. 44, no. 1, pp. 157–164, 2008.

[42] Q. G. Zhao, W. H. Shen, and K. L. Yuan, "Sensitivity of summer rainstorm in Yangtze and Huaihe river valley to large scale humidity fields," *Quarterly Journal of Applied Meteorology*, vol. 6, no. 3, pp. 320–326, 1995.

[43] G. Q. Xu and Y. X. Zhang, "The heavy rain's vapor sources and vapor sensitivity simulation in August 1996," *Meteorological Monthly*, vol. 25, no. 7, pp. 12–16, 1999.

[44] X. R. Zhang, X. R. Li, and Y. F. Liao, "A numerical study on the effect of water vapor on a rainstorm related to shear line during Meiyu period," *Journal of Applied Meteorology and Climatology*, vol. 41, no. 5, pp. 617–630, 2021.

[45] Y. H. Ding, *A Set of Softwares for Mesoscale Diagnosis and Analysis*, China Meteorological Press, Beijing, China, 1996.

[46] J. Liu, X. Y. Shen, and Y. H. Yang, "Numerical sensitivity test on the severe tropical storm Bilis," *Science and Technology Information*, vol. 2, pp. 4–6, 2008.

[47] J. H. Zhang, G. Y. Xue, and H. M. Chen, "Analysis and numerical experiments of the impact of moisture transportation by southwest monsoon on precipitation of the tropical cyclone Bilis," *Science and Technology Review*, vol. 26, no. 23, pp. 74–82, 2008.

[48] Y. S. Zhou, S. T. Gao, and G. Deng, "A diagnostic study of water vapor transport and budget during heavy precipitation over the Changjiang river and the Huaihe river basins in 2003," *Chinese Journal of Atmospheric Sciences*, vol. 29, no. 2, pp. 195–204, 2005.

[49] C. M. Miao, Y. H. Ding, and P. W. Guo, "Linkage of the water vapor transport distribution with the rainy season and its precipitation in the southern regions south of the Yangtze river during the early summer," *Acta Meteorologica Sinica*, vol. 73, no. 1, pp. 72–83, 2015.

[50] Z. M. Kang, "Analysis of moisture transfer associated with sustained heavy rain in 2003 over Jianghuai valley," *Meteorological Monthly*, vol. 30, no. 2, pp. 20–24, 2004.

[51] J. H. He, C. H. Sun, Y. Y. Liu, J. Matsumoto, and W. Li, "Seasonal transition features of large-scale moisture transport in the Asian-Australian monsoon region," *Advances in Atmospheric Sciences*, vol. 24, no. 1, pp. 1–14, 2007.

[52] Z. H. Jiang, Z. R. Liang, and Z. Y. Liu, "A diagnostic study of water vapor transport and budget during heavy precipitation over the Huaihe river basin in 2007," *Chinese Journal of Atmospheric Sciences*, vol. 35, no. 2, pp. 361–372, 2011.

[53] J. F. Su, T. Zhou, B. Zhu, and S. Y. Liu, "Diagnostic analysis on Meiyu rainstorm and its simulation based on backward trajectory analysis method during June 2009 in the south of Anhui province," *Journal of Meteorological Research*, vol. 26, no. 3, 2010.

[54] J. H. Sun, S. X. Zhao, and S. M. Fu, "Multi-scale characteristics of record heavy rainfall over Beijing area on July 21, 2012," *Chinese Journal of Atmospheric Sciences*, vol. 37, no. 3, pp. 705–718, 2013.

[55] Y. Li, W. J. Yuan, and Q. Q. Xu, "Water vapor transportation characteristics in pre-rainy season precipitation anomaly of South China," *Plateau Meteorology*, vol. 36, no. 2, pp. 501–509, 2017.

[56] C. Z. Ye, Y. Y. Li, and Z. X. Li, "Numerical study on the water vapor transports of the two landfalling cyclones affecting Hunan province," *Plateau Meteorology*, vol. 28, no. 1, pp. 98–107, 2009.

[57] J. J. Wang, C. X. Wang, and Z. P. Chen, "Analysis of a summer rainstorm water vapor paths and sources in Sichuan basin based on HYSPLIT4 model," *Meteorological Monthly*, vol. 41, no. 11, pp. 1315–1327, 2015.

[58] Y. Shi, Z. H. Jiang, and Z. X. Li, "Vertical characteristics of water vapor transport during the rainy season in eastern China based on the Lagrangian method," *Chinese Journal of Atmospheric Sciences*, vol. 46, no. 2, pp. 380–392, 2022.

[59] A. Stohl and P. James, "A Lagrangian analysis of the atmospheric branch of the global water cycle. Part I: method description, validation, and demonstration for the August 2002 flooding in central Europe," *Journal of Hydrometeorology*, vol. 5, no. 4, pp. 656–678, 2004.

[60] A. Stohl and P. James, "A Lagrangian analysis of the atmospheric branch of the global water cycle. Part II: moisture transports between earth's ocean basins and river catchments," *Journal of Hydrometeorology*, vol. 6, no. 6, pp. 961–984, 2005.

[61] F. Dominguez, P. Kumar, X. Z. Liang, and M. Ting, "Impact of atmospheric moisture storage on precipitation recycling," *Journal of Climate*, vol. 19, no. 8, pp. 1513–1530, 2006.

[62] P. A. Dirmeyer, C. A. Schlosser, and K. L. Brubaker, "Precipitation, recycling, and land memory: an integrated analysis," *Journal of Hydrometeorology*, vol. 10, no. 1, pp. 278–288, 2009.

[63] L. Gimeno, A. Drumond, R. Nieto, R. M. Trigo, and A. Stohl, "On the origin of continental precipitation," *Geophysical Research Letters*, vol. 37, no. 13, Article ID L13804, 2010.

[64] K. L. Brubaker, P. A. Dirmeyer, A. Sudradjat, B. S. Levy, and F. Bernal, "A 36-yr climatological description of the evaporative sources of warm-season precipitation in the Mississippi river basin," *Journal of Hydrometeorology*, vol. 2, no. 6, pp. 537–557, 2001.

[65] J. E. Diem and D. P. Brown, "Tropospheric moisture and monsoonal rainfall over the southwestern United States," *Journal of Geophysical Research*, vol. 111, no. D16, Article ID D16112, 2006.

[66] A. Bertò, A. Buzzi, and D. Zardi, "Back-tracking water vapour contributing to a precipitation event over Trentino: a case study," *Meteorologische Zeitschrift*, vol. 13, no. 3, pp. 189–200, 2004.

[67] L. B. Perry, C. E. Konrad, and T. W. Schmidlin, "Antecedent upstream air trajectories associated with northwest flow snowfall in the southern Appalachians," *Weather and Forecasting*, vol. 22, no. 2, pp. 334–352, 2007.

[68] H. Sodemann and A. Stohl, "Asymmetries in the moisture origin of Antarctic precipitation," *Geophysical Research Letters*, vol. 36, no. 22, Article ID L22803, 2009.

[69] A. Drumond, J. Marengo, T. Ambrizzi, R. Nieto, L. Moreira, and L. Gimeno, "The role of the Amazon basin moisture in the atmospheric branch of the hydrological cycle: a Lagrangian analysis," *Hydrology and Earth System Sciences*, vol. 18, no. 7, pp. 2577–2598, 2014.

[70] A. A. M. Salih, Q. Zhang, and M. Tjernström, "Lagrangian tracing of Sahelian Sudan moisture sources," *Journal of Geophysical Research: Atmospheres*, vol. 120, no. 14, pp. 6793–6808, 2015.

[71] R. R. Draxler and G. D. Hess, "An overview of the HYSPLIT_4 modeling system for trajectories, dispersion and deposition," *Australian Meteorological Magazine*, vol. 47, pp. 295–308, 1998.

[72] Y. Shi, Z. H. Jiang, Z. Y. Liu, and L. Li, "A Lagrangian analysis of water vapor sources and pathways for precipitation in east China in different stages of the east Asian summer monsoon," *Journal of Climate*, vol. 33, no. 3, pp. 977–992, 2020.

[73] B. Sun and H. J. Wang, "Moisture sources of semiarid grassland in China using the Lagrangian particle model FLEXPART," *Journal of Climate*, vol. 27, no. 6, pp. 2457–2474, 2014.

[74] B. Sun and H. J. Wang, "Analysis of the major atmospheric moisture sources affecting three sub-regions of East China," *International Journal of Climatology*, vol. 35, no. 9, pp. 2243–2257, 2015.

[75] Y. C. Lin, T. J. Wei, and D. C. Jiang, *Synoptic Experiment and Diagnostic Analysis*, Nanjing University Press, Nanjing, China, 1991.

[76] Q. G. Zhu, *Synoptic Principles and Methods*, Meteorological Press, Beijing, China, 2000.

[77] Y. Du, Y. C. Zhang, and Z. Q. Xie, "Impacts of longitude location changes of East Asia westerly jet core on the precipitation distribution during Meiyu period in middle-lower reaches of Yangtze river valley," *Acta Meteorologica Sinica*, vol. 66, no. 4, pp. 566–576, 2008.

[78] X. Lai, Y. Gong, S. Cen, H. Tian, and H. Zhang, "Impact of the westerly jet on rainfall/runoff in the source region of the Yangtze river during the flood season," *Advances in Meteorology*, vol. 2020, Article ID 6726347, 11 pages, 2020.

[79] J. Zheng, S. Sun, J. Wu, and A. H. Xu, "Analysis on multi-scale ambient field for short-time severe torrential rain on Meiyu front," *Meteorological Monthly*, vol. 40, no. 5, pp. 570–579, 2014.

[80] H. Li, Y. Hu, Z. Zhou, J. Peng, and X. D. Xu, "Characteristic features of the evolution of a Meiyu frontal rainstorm with doppler radar data assimilation," *Advances in Meteorology*, vol. 2018, Article ID 9802360, 17 pages, 2018.

[81] R. A. Maddox, "Meoscale convective complexes," *Bulletin America Meteorology Social*, vol. 61, no. 11, pp. 1374–1387, 1980.

[82] F. F. Wu, X. D. Yu, H. Wang, J. Shang, and W. J. Zhou, "An observational study of multi-scale structural features of MCC on the coast of the yellow sea," *Acta Meteorologica Sinica*, vol. 77, no. 5, pp. 785–805, 2019.